# Diffusion-Weighted MRI as a Biomarker of Tumor Radiation Treatment Response Heterogeneity: A Comparative Study of Whole-Volume Histogram Analysis *versus* Voxel-Based Functional Diffusion Map Analysis[1]

Benjamin Lemasson*, Craig J. Galbán*, Jennifer L. Boes*, Yinghua Li[†], Yuan Zhu[†], Kevin A. Heist*, Timothy D. Johnson[‡], Thomas L. Chenevert*, Stefanie Galbán[§], Alnawaz Rehemtulla[§] and Brian D. Ross*

*Department of Radiology, University of Michigan, Ann Arbor, MI; [†]Department of Internal Medicine, University of Michigan, Ann Arbor, MI; [‡]Department of Biostatistics, University of Michigan, Ann Arbor, MI; [§]Department of Radiation Oncology, University of Michigan, Ann Arbor, MI

## Abstract

*RATIONALE:* Treatment of glioblastoma (GBM) remains challenging due in part to its histologic intratumoral heterogeneity that contributes to its overall poor treatment response. Our goal was to evaluate a voxel-based biomarker, the functional diffusion map (fDM), as an imaging biomarker to detect heterogeneity of tumor response in a radiation dose escalation protocol using a genetically engineered murine GBM model. *EXPERIMENTAL DESIGN:* Twenty-four genetically engineered murine GBM models [Ink4a-Arf$^{-/-}$/Pten$^{loxp/loxp}$/Ntv-a RCAS/PDGF(+)/Cre(+)] were randomized in four treatment groups ($n = 6$ per group) consisting of daily doses of 0, 1, 2, and 4 Gy delivered for 5 days. Contrast-enhanced T1-weighted and diffusion-weighted magnetic resonance imaging (MRI) scans were acquired for tumor delineation and quantification of apparent diffusion coefficient (ADC) maps, respectively. MRI experiments were performed daily for a week and every 2 days thereafter. For each animal, the area under the curve (AUC) of the percentage change of the ADC (AUC$_{ADC}$) and that of the increase in fDM values (AUC$_{fDM+}$) were determined within the first 5 days following therapy initiation. *RESULTS:* Animal survival increased with increasing radiation dose. Treatment induced a dose-dependent increase in tumor ADC values. The strongest correlation between survival and ADC measurements was observed using the AUC$_{fDM+}$ metric ($R^2 = 0.88$). *CONCLUSION:* This study showed that the efficacy of a voxel-based imaging biomarker (fDM) was able to detect spatially varying changes in tumors, which were determined to be a more sensitive predictor of overall response *versus* whole-volume tumor measurements (AUC$_{ADC}$). Finally, fDM provided for visualization of treatment-associated spatial heterogeneity within the tumor.

*Translational Oncology* (2013) 6, 554–561

## Introduction

Glioblastoma (GBM) is the most common and malignant form of primary brain tumor in adults [1]. Standard therapy for treating patients with GBM is a combination of maximal safe surgical resection with chemotherapy and radiotherapy [2,3]. The prognosis for patients with GBM is generally poor with an average survival time of 51 weeks [4]. Assessment of response to therapy is based on the measurement of the tumor size 8 to 10 weeks after the start of treatment [5]. Because of poor patient outcomes associated with limited

Address all correspondence to: Brian D. Ross, PhD, Center for Molecular Imaging, University of Michigan, Biomedical Sciences Research Building, Room 2071, 109 Zina Pitcher Place, Ann Arbor, MI 48109-2200. E-mail: bdross@umich.edu

survival time, there is a clinical need for the development of quantitative imaging biomarkers that can provide early stratification of treatment efficacy.

Magnetic resonance imaging (MRI) is able to noninvasively acquire a wide range of brain tumor characteristics (morphologic and physiological) and has become the technique of choice for assessing therapeutic response [6]. MRI is routinely employed to estimate tumor volume using anatomic images but also tumor-associated edema and tumor cellularity using the apparent diffusion coefficient (ADC) of water calculated using diffusion-weighted (DW) MRI sequences [7–10]. Diffusion imaging has been successfully used to assess glioma response to different chemotherapies [9,11,12] as well as radiotherapy [12]. Taken together, these studies have shown that DW-MRI is a sensitive biomarker that is capable of detecting early cellular changes in treated tumors, which precede macroscopic volumetric response. Whole-tumor analysis is the most common technique for assessing therapeutic response, typically comparing differences in mean tumor ADC values post-therapy (or mid-therapy) to the pretherapy values. However, several studies have shown that diffusion changes could both increase and decrease over time within the same tumor, which is a consequent of the highly heterogeneous response of GBMs to treatment [13–15]. Assessing the mean change in overall tumor ADC value can lead to a diminution of sensitivity of the ADC measure because of divergent (increase/decrease) changes in tumor ADC values in response to treatment.

Assessing therapeutic response in patients with glioma using ADC maps observed that tumor reaction to cytotoxic treatment was spatially dependent [14]. This led our group to develop the first voxel-based approach called the functional diffusion map (fDM) using registered longitudinal diffusion ADC maps [14–16]. The voxel-by-voxel analysis approach has distinct advantages over whole-tumor volume techniques such as histogram analysis, as it allows for classification of individual tumor voxels based on the extent of change in ADC values during therapy [14]. We have demonstrated the efficacy of fDM as an early surrogate biomarker of survival in brain tumor as well as in the 9L rodent glioma model undergoing chemotherapy [15,16].

In the current study, whole-tumor volume percent change in mean ADC values was compared with fDM metrics following radiation treatment using a genetically engineered murine GBM model to evaluate these approaches as imaging biomarkers of tumor response. The GBM model was found to have a heterogeneous pattern of response similar to that observed in clinical subjects, where regions within the tumor increased and decreased in ADC values during treatment. Compared to the histogram-based approach, the fDM biomarker was determined to provide the most predictive metric correlated to overall survival following radiation therapy and in a dose-dependent manner. Overall, the fDM biomarker approach has potential broad applications in both preclinical drug development settings as well as for translational clinical trials and individualized patient management.

## Materials and Methods

### Cell Culture

DF-1 cells were purchased from ATCC (Manassas, VA). Cells were grown at 39°C according to ATCC instructions. RCAS–PDGF-B–HA and RCAS-Cre, provided by Dr E. Holland, have been described previously [15,17–19]. Transfections with RCAS–PDGF-B–HA or RCAS-Cre were performed using FuGENE 6 transfection kit according to the manufacturer's instructions (Roche Applied Science, Indianapolis, IN). Expression of PDGF and Cre was confirmed by Western blot analysis of the HA-HRP antibody (Sigma, St Louis, MO) and Cre (Berkeley Antibody, Richmond, CA).

### Intracranial Inoculation

The University of Michigan Laboratory Animal (ULAM) Committee approved the use of animals for this study. Generation of the Nestin-tv-a, Ink4a-Arf$^{-/-}$, Pten$^{loxp/loxp}$ mouse lines has previously been described [15–19]. Animals were originally acquired from E. Holland and inbred at the University of Michigan ULAM facility. Intracranial inoculation was performed on 4- to 6-week-old transgenic mice (Nestin-tv-a, Ink4a-Arf$^{-/-}$, Pten$^{loxp/loxp}$). Mice were anesthetized with a ketamine/xylazine (0.1/0.02 mg/kg) mixture and prepped with topical antiseptic before cell injection. A 1-μl suspension containing 8 × $10^4$ cells with an equal number of RCAS–PDGF-B– and RCAS-Cre–transfected DF1 cells was delivered using a 30-gauge needle attached to a Hamilton syringe and stereotactic fixation device (Stoelting, Wood Dale, IL) at coordinates of 1.5 mm (bregma) and 0.5 mm (lateral) and a depth of 1.5 mm.

### Treatment

Following intracranial inoculation, tumor volumes were monitored over time using contrast-enhanced (CE) T1-weighted MRI as described below. Once tumor volumes reached 20 to 40 mm$^3$, pre-treatment MRI images were acquired and treatment was initiated on day 0. Animals ($n$ = 40) were randomized into four different groups ($n$ = 10 per group) as follows: sham-treated (0 Gy) and 5, 10, and 20 Gy total ionizing radiation (IR) doses that were delivered by fractionated doses over a 5-day period (0, 1, 2, and 4 Gy/day, respectively). Through the duration of the study, several of the mice encountered untimely attrition unrelated to treatment or tumor growth. Mice were sacrificed when they became moribund or tumor size exceeded 200% of their baseline volume (20-40 mm$^3$).

### MRI Scans

MRI scans were performed on a 9.4-T, 16-cm horizontal bore (Agilent Technologies, Inc, Santa Clara, CA) Direct Drive System with a mouse head quadrature volume coil (m2m Imaging, Corp, Cleveland, OH) or mouse surface receive coil actively decoupled to a whole-body volume transmit coil (RAPID MR International, LLC, Columbus, OH). Throughout the MRI experiments, animals were anesthetized with 1% to 2% isoflurane/air mixture, and body temperature was maintained using a heated air system (Air-Therm Heather; World Precision Instruments, Sarasota, FL).

MRI was performed on mice to quantify tumor volumes over time along with tumor water diffusion values. Delineation of tumor tissue from healthy brain was accomplished using CE T1-weighted spin-echo MRIs with the following parameters: repetition time/echo time = 510/15 ms, field of view = 20 × 20 mm$^2$, matrix size = 128 × 128, slice thickness = 0.5 mm, 25 slices, and two averages. Total acquisition time was 2 minutes and 12 seconds. Contrast enhancement was performed by i.p. administration of 50 μl of 0.5 M gadolinium-DTPA (Magnevist; Bayer Healthcare Pharmaceuticals, Wayne, NJ) 5 minutes before acquisition initiation. Tumor ADC maps were obtained from a diffusion-weighted spin-echo sequence, equipped with a navigator echo for motion correction and gradient waveforms sensitive to isotropic diffusion, with the following parameters: repetition time/echo time = 2000/37 ms,

field of view = $20 \times 20$ mm$^2$, matrix size = $128 \times 64$, slice thickness = 0.5 mm, 25 slices, two averages, diffusion time = 40 ms, gradient pulse width = 10 ms, and $b$ values (diffusion weighting) of 0, 120, and 1200 s/mm$^2$. Total acquisition time was 8 minutes and 32 seconds.

CE-MRI and DW-MRI were acquired daily between day 0 and day 5 for all animals under study. At day 5, four animals per group were sacrificed following the MRI session for histology (see below). The 24 remaining animals (six per group) were monitored by CE-MRI every other day to quantify tumor volume changes over time.

### Image Reconstruction and Analyses

Tumors were manually contoured along the enhancing rim of the tumors on the CE T1-weighted images. These tumor volumes of interest were used to calculate tumor volume and whole-tumor means of ADC and delineate the tumor volume for fDM analysis.

ADC maps were calculated from the two diffusion-weighted images using the following equation:

$$ADC = \ln\left(\frac{S_1}{S_2}\right) / (b_2 - b_1),$$

where $S_1$ and $S_2$ are the diffusion-weighted images at $b$ values $b_1$ and $b_2$, respectively, and ADC is the apparent diffusion coefficient obtained using $b_1$ and $b_2$. All image reconstruction and digital image analyses were accomplished using in-house programs developed in Matlab (The Mathworks, Natick, MA).

In brief, fDM analysis was accomplished in the following three steps: computation of temporally resolved quantitative ADC maps, image registration of serial ADC maps followed by classification of voxel-based ADC changes based on predetermined thresholds. Mid-treatment CE images and all ADC maps were spatially aligned to the pre-treatment CE image using a stepwise image registration approach. Initial registration of serial MRI scans to the baseline scan (day 0) was performed assuming a rigid-body geometry relationship to provide for rapid alignment of the head using an initial set of four control points. Next, images were co-registered using a thin-plate spline transformation that was optimized using mutual information as an objective function and Nelder-Mead simplex as an optimizer [20]. This process required an additional set of control points that were automatically placed within the tumor volume based on the size and information content of the tumor. Degrees of freedom of the final transform were 36 to 72.

The fDM data were determined by first calculating the difference between the ADC within the tumor before therapy and at each mid-treatment time point. Red voxels represent the tumor volume where ADC value increased beyond the user-defined ADC threshold of $0.2 \times 10^{-3}$ mm$^2$/s (described below), blue voxels represent volumes whose ADC decreased by more than $0.20 \times 10^{-3}$ mm$^2$/s, and the green voxels represent voxels within the tumor that were unchanged (that is, the absolute value of $\Delta$ADC was $<0.20 \times 10^{-3}$ mm$^2$/s). All voxels within a classification were summed and normalized to total tumor volume to generate three volume fractions: fDM+ (increased ADC, denoted red), fDM− (decreased ADC, denoted blue), and fDM0 (unchanged ADC, denoted green). Calculation of the fDM thresholds for voxel classification has been previously described [21]. Briefly, we empirically calculated the thresholds that designate a significant change in ADC within a voxel from five untreated tumors. For each animal, we used the tumor region of interest before and 1 day after therapy initiation. Combining the data from all five subjects, we

performed linear least-squares regression analysis on the pre-treatment and intra-treatment ADC values. We then determined the 95% confidence intervals from the resulting linear least-squares analysis. The threshold obtained was $0.20 \times 10^{-3}$ mm$^2$/s (data not shown).

In addition to analyzing the metrics at each time point, the area under the curve (AUC) between day 0 and day 5 (24 hours after the last therapy) were calculated for both the percentage change of ADC (AUC$_{ADC}$) and for the fDM metrics (AUC$_{fDM}$).

### Immunohistochemistry

For each of the treatments, three animals from each group were sacrificed at day 5 (24 hours after the last treatment), and tumors were harvested and fixed in 10% neutral buffered formalin for at least 48 hours. Tumors were sectioned and paraffin embedded, and 5-µm sections were cut onto slides. Paraffin was removed in xylene, and slides were rehydrated through gradually decreasing alcohol concentrations 2 min/step before ending in tap water (100% ethanol, 95% ethanol, 70% ethanol, water). The slides were stained with H&E (cell viability), Ki-67 antibody (cell proliferation), and ApopTag (apoptosis) after antigen retrieval with Diva (Biocare, Concord, CA) using the Avidin/Biotin Complex System (Vectastain; Vector Labs, Burlingame, CA) and discolored with the DAB solution (Vector Labs).

Nontreated or treated brain tumor sections were imaged at the same magnification using an Olympus microscope and subjected to quantitative analysis. Because of the heterogeneous nature of the tumors, Ki-67 and apoptosis indices were quantified using the highest staining area. Briefly, staining was checked under low magnification, and then the highest staining area was identified. The image was taken at ×80, and then Ki-67–positive or ApopTag+ cells and total cells were counted by ImageJ.

### Statistics

Overall survival of the treatment groups was assessed by log-rank tests and Kaplan-Meier survival curves. Group comparisons of MRI and immunohistologic results were determined at individual time points using analysis of variance (ANOVA) and least-squares difference to correct for multiple comparisons. A Pearson correlation analysis was used to determine linear relationships between imaging biomarkers and overall survival. Immunologic differences between groups were assessed using two-tailed Student's $t$ test in Prism 6 (GraphPad Software, Inc, La Jolla, CA). All other statistical computations were performed with a statistical software package (SPSS Software Products, Chicago, IL). Statistical significance was assessed at $P < .05$. All results were presented as means ± SEM.

## Results

### Survival and Tumor Growth

A Kaplan-Meier survival plot for all treatment groups revealed a dose-dependent increase in animal survival (Figure 1A). All groups were found to have significantly different survival post-therapy ($P < .05$). The median survival time of untreated (0 Gy) and 1, 2, and 4 Gy groups was 3.6 ± 0.2, 7.2 ± 1.2, 13.8 ± 1.5, and 21.5 ± 1.5 days, respectively (Figure 1A).

A plot of the percentage change in tumor volumes for all groups as a function of time post-treatment initiation is presented in Figure 1B. The volume of untreated tumors increased rapidly and by day 4
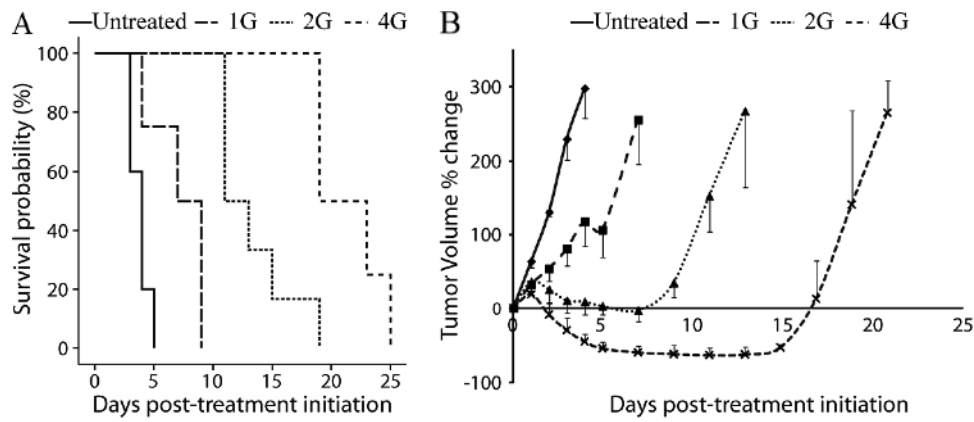
**Figure 1.** (A) Kaplan-Meier survival plots are presented for each therapy (0, 1, 2, and 4 Gy). The median survival for these groups was 4, 7, 11, and 19 days post-therapy, respectively. All groups were significantly different, as determined by log-rank test ($P < .05$). (B) Percentage change of tumor volumes for 0, 1, 2, and 4 Gy groups assessed by MRI as a function of time. Data are presented as the means $\pm$ SEM.

reached the criteria for removal from the study (260 $\pm$ 33%). At 2 days post-treatment initiation, the percentage change of the tumor size of the untreated group was significantly higher compared to all the treated groups (129 $\pm$ 6% *versus* 53.5 $\pm$ 18%, 31.5 $\pm$ 22%, and –9 $\pm$ 8% for the untreated and 1, 2, and 4 Gy groups, respectively; $P < .05$). The percentage change of tumor size of the 1 Gy group was statistically different from all other treatment groups at day 4 (117 $\pm$ 33% *versus* 14 $\pm$ 20% and –46 $\pm$ 5% for the 1 Gy *versus* 2 and 4 Gy groups, respectively;
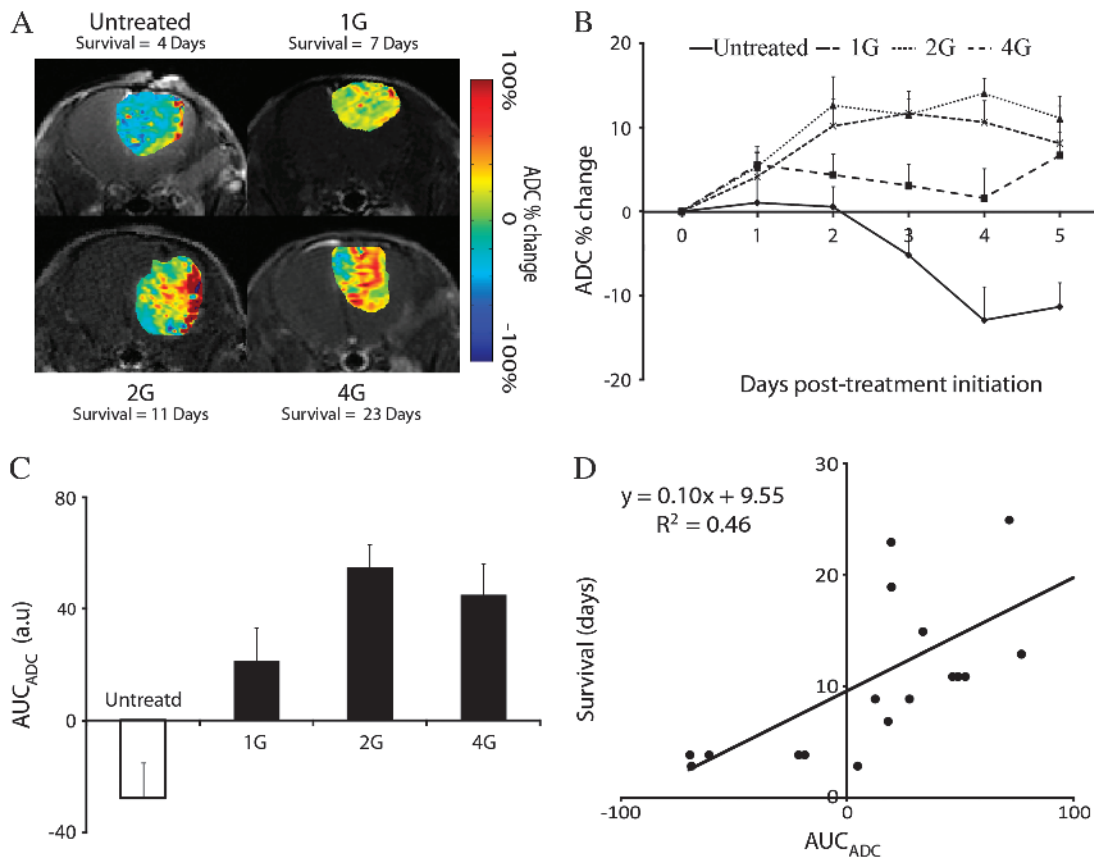


**Figure 2.** (A) Representative MRIs of each group acquired at time of maximum percentage change in mean ADC. The times were day 4 and day 7, day 11, and day 23 for untreated and 1, 2, and 4 Gy, respectively. MRI data consist of ADC percent change images (color maps) overlaid on the anatomic CE T1-weighted images. ADC percent change images were generated by calculating the percentage change of ADC values on a voxel-by-voxel basis using registered mid-treatment and pre-therapy ADC maps. (B) Plots of the percentage change in ADC as a function of time for each treatment group. (C) AUC of the percentage change in ADC measured during the therapy (day 0 to day 5) for each treatment group (means $\pm$ SD). All groups were significantly different, as determined by ANOVA followed by an Least Significance Difference (LSD) correction test ($P < .05$). (D) Scatter plot and linear regression of the AUC of the percentage change of ADC value measured during the therapy (day 0 to day 5) as a function of the overall survival. Each dot represents an individual animal. Data are presented as the means $\pm$ SEM.

$P < .05$). In addition, the 2 and 4 Gy doses were also significant from each other at day 4 ($P < .05$).

### Treatment-Induced Percentage Change in Tumor ADC Values

We observed large spatial variation in tumor ADC values at peak response (i.e., maximum percentage change in mean ADC) for each group post-treatment initiation (Figure 2A). When analyzing the whole-tumor ADC metric at each time point, the percentage change in mean ADC values in the 2 and 4 Gy groups were significantly higher than the untreated group 2 days post-treatment initiation ($12.1 ± 3.1\%$ and $10.2 ± 3.3\%$ *versus* $0.6 ± 2.4\%$, respectively, $P < .05$; Figure 2B). By day 3, the percentage change in tumor ADC values increased significantly in the 1 Gy group compared to the untreated group ($3.1 ± 2.6\%$ *versus* $–5.2 ± 3.2\%$, $P < .05$; Figure 2B). Despite the elevated ADC values from baseline in the 2 Gy group over the 4 Gy treated group, no significant differences were observed (Figure 2B). All treated groups generated $AUC_{ADC}$ values that were significantly higher than the untreated group ($–27.8 ± 15.5\%$ *versus* $23.0 ± 12.9\%$, $52.8 ± 8.4\%$, and $44.7 ± 11.3\%$, for the untreated and 1, 2, and 4 Gy groups, respectively, $P < .05$; Figure 2C). In addi-tion, $AUC_{ADC}$ correlated with overall survival ($R^2 = 0.46$, $P = .002$; Figure 2D).

### The fDM as an Imaging Biomarker of Survival

Analysis by fDM of the same representative animals displayed in Figure 2 showed regions of tumor with elevated ADC values from baseline that increased with radiation dose [Figure 3A; red voxels (fDM+)]. Although the number of fDM+ voxels in the 1 Gy group were higher than the untreated group at each of the time points, this difference was not significant with near significance occurring at day 5 ($1.6 ± 0.4$ *versus* $11.3 ± 2.0$, for the untreated and 1 Gy groups, respectively, $P = .055$; Figure 3B). When compared to untreated animals, significant differences in fDM+ for 2 and 4 Gy groups were observed as early as day 2 ($2.5 ± 0.6\%$ *versus* $12.7 ± 4.5\%$, $P < .05$) and day 1 ($2.2 ± 085\%$ *versus* $7.1 ± 2.5\%$, $P < .05$), respectively. Despite the fact that for all time points the fDM+ values of the 4 Gy group were higher than those measured in the 2 Gy group, significant differences were observed at day 1 and day 3 only ($7.1 ± 2.5\%$ *versus* $2.0 ± 0.7\%$ and $22.7 ± 3.2\%$ *versus* $9.5 ± 1.7\%$, respec-tively; Figure 3B). We observed an increase of $AUC_{fDM+}$ values in a
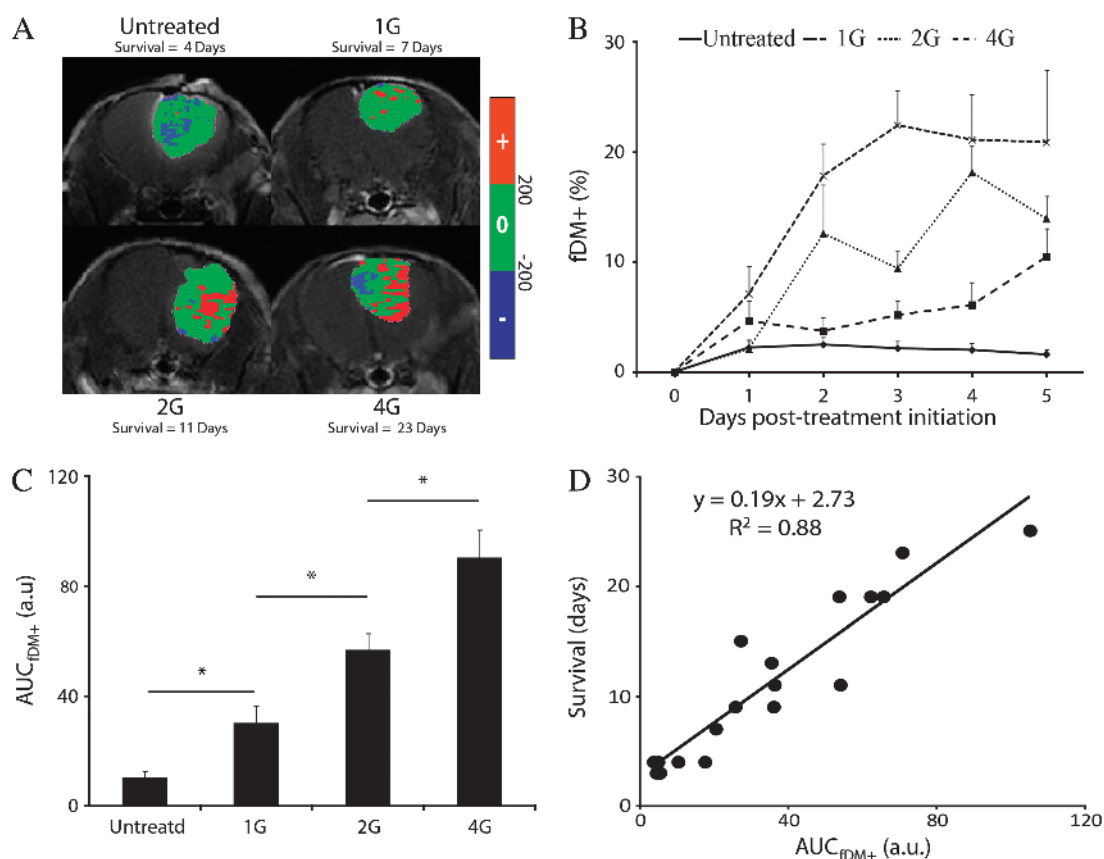


**Figure 3.** (A) fDM overlays of the same representative animals and time points used in Figure 2A. fDM images (color maps) are overlaid on anatomic CE T1-weighted images. Images of fDMs reveal red voxels, which are regions with significant increases in ADC, and blue voxels, which are regions within the tumor with significantly decreased ADC values. The green voxels are tumor regions wherein the ADC values did not change (over the defined threshold level of $±0.2 × 10^{-9}$ m$^2$/s). (B) Plots of the fDM increases (fDM+) as a function of time for each treatment group. Data are presented over the first 5 days of treatment as the means $±$ SD. (C) AUC of the fDM+ measured during the therapy (day 0 to day 5) for each treated group (means $±$ SD). All groups were significantly different, as determined by ANOVA followed by an LSD correction test ($P < .05$). (D) Scatter plot and linear regression of the AUC of the fDM+ value measured during the therapy (day 0 to day 5) as function of the overall survival. Each dot represents an individual animal. Data are presented as the means $±$ SEM.
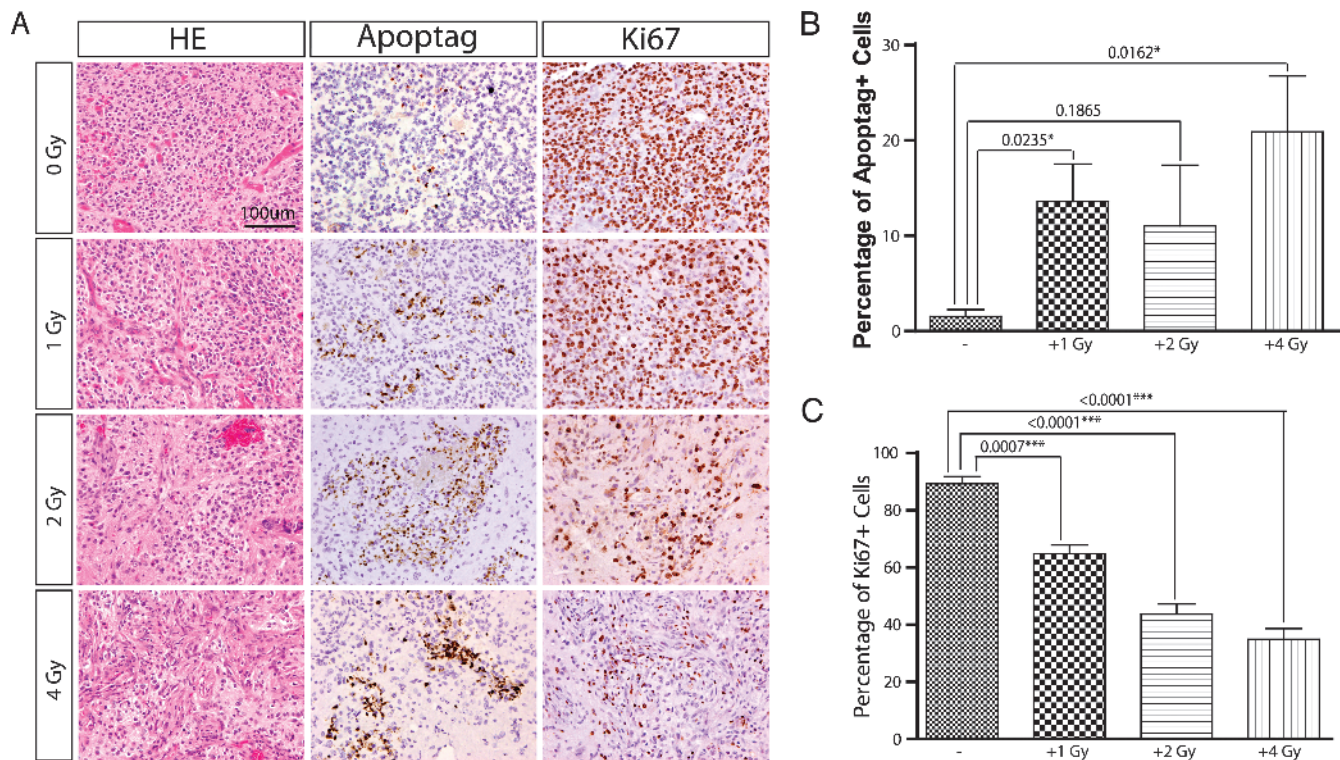
**Figure 4.** Dose-dependent response of IR treatment. (A) Representative images showing the proliferation and apoptosis of tumor cells under different dose of IR treatment. (B) The percentage of apoptotic cells (ApopTag+) was quantified (40× area) among different doses of IR treatments (mice of each group: $n$ = 3). (C) The percentage of proliferative cells (Ki-67+) were quantified (40× area) among different doses of IR treatments (mice of each group: $n$ = 3). Data are presented as the means ± SEM.

radiation dose–dependent way (10.6 ± 2.1%, 33.4 ± 8.7%, 56.7 ± 6.2%, and 90.4 ± 10.1% for the 0, 1, 2, and 4 Gy, respectively; Figure 3C). $AUC_{fDM+}$ was statistically different between each group ($P < .05$; Figure 3C) with a strong correlation to overall survival ($R^2$ = 0.88, $P = 9.3 \times 10^{-8}$; Figure 3D).

### Immunohistochemical Evaluation of In Vivo GBM Treatment Effects

To study the effects of radiation dose on tumor cell morphology, proliferation, and apoptosis, intracranial tumors harvested at day 5 (24 hours after the last treatment) were subjected to immunohistochemical analysis. Tumors displayed findings similar to human GBM, including nuclear atypia, mitotic figures, areas of necrosis, and vascular/endothelial proliferation (Figure 4A). Untreated tumors displayed low percentage of apoptotic cells (Figure 4B). We observed an increase in apoptotic cells in the three treated groups compared to the untreated group (Figure 4, A and B). In contrast, a significant dose-dependent decrease in tumor proliferation, as measured by Ki-67, was observed in each of the treated groups compared to untreated animals (Figure 4, A and C).

### Discussion

High-grade gliomas are markedly heterogeneous in their morphologic and genetic nature. As such, they demonstrate a spatially heterogeneous response to cytotoxic and radiation therapies with tumor regions developing elevated levels of edema, necrosis, and angiogenesis adding difficulty in ascertaining treatment efficacy. Advanced quantitative MRI techniques, such as DW-MRI, have shown promise as a robust approach for response monitoring of tumors by focusing on a specific feature of the tumor, in this case tumor cellularity. Although physiological changes within the tumor following therapy can be visualized by quantitative MRI, the use of these techniques as a surrogate biomarker of patient survival continues to be hampered due to uncertainties in knowing how to optimally analyze the data to provide for the most predictive metric [8].

The traditional method of analyzing quantitative images is to calculate a scalar quantity, i.e., mean or median, that represents the physiological state of the entire tumor volume at a given time point. A positive or negative response of the tumor following a therapeutic intervention can be inferred from the percentage change in the quantitative scalar value, thus providing a biomarker for patient survival prediction that can be used as a surrogate to a meaningful clinical end point. Although this technique can be applied quickly and easily by simply contouring the tumor volume, in our study this metric yielded only a limited correlation with overall survival. Statistical-based approaches that rely on whole-tumor values may not provide enough sensitivity for detection of treatment-induced changes when the underlying changes within the tumor mass are heterogeneous, which results in attenuation of the biomarker metric, thus hampering detection of overall therapeutic response.

However, voxel-based approaches that employ a classification scheme, i.e., fDM, provide a unique opportunity to fully use the morphologic information contained within the temporally resolved quantitative maps, i.e., ADC, for response assessment. The fact that fDM can separate the response heterogeneity within the tumor into

discrete classes of increased, decreased, or unchanged ADC values eliminates the attenuation that typically occurs in whole-tumor analysis approaches. Moreover, the fDM approach also allows delineation of the most predictive response metric, which for fDM is the relative tumor volume with increasing ADC (fDM+). Through voxel-based techniques, individual classifications can each be thoroughly evaluated as predictive biomarkers, each of which provides distinctive information related to the morphologic or physiological changes occurring within the tumor mass during therapy [14,16,21–23].

In the present study, we report only a 10% increase in the percentage change of tumor ADC following 2 and 4 Gy doses with little to no difference between these groups (Figure 2B). Although consistent with previous studies [15,24,25], the weak correlation between the whole-tumor ADC metric and overall survival (Figure 2D) was attributed to the tumor response heterogeneity in the GBM model. In contrast, applying fDM to the ADC maps and focusing on the most robust response metric, i.e., fDM+, we were able to improve our detection of dose-dependent trends in tumor response (Figures 2B and 3B). Calculation of AUC of fDM over the 5-day fractionated therapy was also found to be strongly correlated to overall survival (Figure 3D) as well as generating dose-dependent trends (Figure 3C) that were inversely related to those observed in the tumor proliferative potential as determined by Ki-67 staining (Figure 4C). We have reported previously similar correlations between fDM and histologic findings [15,19].

A vital part of fDM is the use of image co-registration. Deformable registration was performed in this study to spatially align temporally resolved MRI data, CE-MRI and ADC maps, for fDM analysis. Imaging data were acquired as late as 5 days post-treatment initiation. As observed in Figure 1B, significant changes in tumor volume had occurred over this time period with volumes increasing up to 300% for untreated animals and decreasing by up 50% for 4 Gy treated animals. However, fDM voxel–based analysis can still be used effectively, as it is not necessary to assume that tumor cells within a given voxel pre-treatment are the same at a later time interval, but rather like structures exist pre-treatment and mid-treatment, which can be used to align and register regions spatially within the tumor mass during therapeutic intervention. The registration algorithm employed in this study uses mutual information as the objective function, thus like structures within image data sets drive the registration of the data between interval scans even in the presence of large volumetric changes. If serial data were misregistered or random, fDM results would correspondingly be erroneous, thus correlation of the fDM+ biomarker metric to response would be unlikely to be observed. In fact, in this study, we found a stronger outcome correlation with fDM+ (Figure 3D) versus whole-volume tumor averages (Figure 2D). Moreover, the quantified histologic data also support the underlying changes in tumor diffusion values (Figure 4). These data reveal the robust and accurate nature of voxel-based longitudinal measures for use in image analysis for the purpose of detecting spatially varying treatment effects.

It is known that genotypic and phenotypic diversities within a tumor mass can greatly influence its growth and response to therapy [26]. Imaging biomarkers such as fDM have the potential to provide rapid and objective/quantitative information related to tumor treatment response. Spatial variations with respect to tumor sensitivity to a treatment intervention would be anticipated to be observable by the fDM biomarker. Red-encoded voxels would indicate regions within the tumor that are responding, whereas green/blue voxels

would be anticipated to be regions that are unresponsive. Spatially distinctive regions exhibiting either up-front resistance or rapid emergence of a resistant cell population can potentially be detectable using the fDM biomarker. In fact, DW-MRI has been shown to be sensitive enough to detect real-time emergence of resistance in an animal tumor model [27]. Further validation of the fDM imaging biomarker will be required for determining the net impact of delineating spatially varying treatment-associated changes in tumor structure and function. However, it is reasonable to assume that the use of voxel-based biomarkers will advance our ability to more effectively treat patients with cancer.

In summary, we demonstrated that MR diffusion imaging, when analyzed using a voxel-based technique, was more sensitive than whole-tumor histogram-based metrics for assessing tumor tissue changes induced by fractionated doses of ionizing radiation. Moreover, this study showed that the efficacy of a voxel-based imaging biomarker (fDM) was able to detect spatially varying changes in tumors that were determined to be a more sensitive predictor of overall response versus whole-tumor measurements (AUC$_{ADC}$). DW-MRI and associated fDMs provide for visualization of treatment-associated intratumoral spatial heterogeneity in both preclinical and clinical studies [14–16,23,28–31]. Possible future uses of fDM include adaptive conformal targeting of external beam ionizing radiation to specific tumor regions exhibiting resistance or spatial guidance of drug injections. Overall, the application of voxel-based analysis provides for both improved sensitivity for detection of changes and three-dimensionally spatially resolved readouts of treatment-associated changes, which is anticipated to improve patient outcomes.

## References

[1] Bondy ML, Scheurer ME, Malmer B, Barnholtz-Sloan JS, Davis FG, Il'yasova D, Kruchko C, McCarthy BJ, Rajaraman P, Schwartzbaum JA, et al. (2008). Brain tumor epidemiology: consensus from the Brain Tumor Epidemiology Consortium. *Cancer* **113**, 1953–1968.

[2] Stupp R, Hegi ME, Mason WP, van den Bent MJ, Taphoorn MJ, Janzer RC, Ludwin SK, Allgeier A, Fisher B, Belanger K, et al. (2009). Effects of radiotherapy with concomitant and adjuvant temozolomide versus radiotherapy alone on survival in glioblastoma in a randomised phase III study: 5-year analysis of the EORTC-NCIC trial. *Lancet Oncol* **10**, 459–466.

[3] Stupp R, Mason WP, van den Bent MJ, Weller M, Fisher B, Taphoorn MJ, Belanger K, Brandes AA, Marosi C, Bogdahn U, et al. (2005). Radiotherapy plus concomitant and adjuvant temozolomide for glioblastoma. *N Engl J Med* **352**, 987–996.

[4] Jansen M, Yip S, and Louis DN (2010). Molecular pathology in adult gliomas: diagnostic, prognostic, and predictive markers. *Lancet Neurol* **9**, 717–726.

[5] Wen PY, Macdonald DR, Reardon DA, Cloughesy TF, Sorensen AG, Galanis E, Degroot J, Wick W, Gilbert MR, Lassman AB, et al. (2010). Updated response assessment criteria for high-grade gliomas: response assessment in Neuro-Oncology Working Group. *J Clin Oncol* **28**, 1963–1972.

[6] Preusser M, de Ribaupierre S, Wohrer A, Erridge SC, Hegi M, Weller M, and Stupp R (2011). Current concepts and management of glioblastoma. *Ann Neurol* **70**, 9–21.

[7] Ross BD, Moffat BA, Lawrence TS, Mukherji SK, Gebarski SS, Quint DJ, Johnson TD, Junck L, Robertson PL, Muraszko KM, et al. (2003). Evaluation of cancer therapy using diffusion magnetic resonance imaging. *Mol Cancer Ther* **2**, 581–587.

[8] Cha S (2009). Neuroimaging in neuro-oncology. *Neurotherapeutics* **6**, 465–477.

[9] Lemasson B, Christen T, Tizon X, Farion R, Fondraz N, Provent P, Segebarth C, Barbier EL, Genne P, Duchamp O, et al. (2011). Assessment of multiparametric MRI in a human glioma model to monitor cytotoxic and anti-angiogenic drug effects. *NMR Biomed* **24**, 473–482.

[10] Barajas RF, Rubenstein JL, Chang JS, Hwang J, and Cha S (2010). Diffusion-weighted MR imaging derived apparent diffusion coefficient is predictive of

clinical outcome in primary central nervous system lymphoma. *AJNR Am J Neuroradiol* **31**, 60–66.

[11] Hall DE, Moffat BA, Stojanovska J, Johnson TD, Li Z, Hamstra DA, Rehemtulla A, Chenevert TL, Carter J, Pietronigro D, et al. (2004). Therapeutic efficacy of DTI-015 using diffusion magnetic resonance imaging as an early surrogate marker. *Clin Cancer Res* **10**, 7852–7859.

[12] Galbán S, Lemasson B, Williams TM, Li F, Heist KA, Johnson TD, Leopold JS, Chenevert TL, Lawrence TS, Rehemtulla A, et al. (2012). DW-MRI as a biomarker to compare therapeutic outcomes in radiotherapy regimens incorporating temozolomide or gemcitabine in glioblastoma. *PLoS One* **7**, e35857.

[13] Chenevert TL, Stegman LD, Taylor JM, Robertson PL, Greenberg HS, Rehemtulla A, and Ross BD (2000). Diffusion magnetic resonance imaging: an early surrogate marker of therapeutic efficacy in brain tumors. *J Natl Cancer Inst* **92**, 2029–2036.

[14] Moffat BA, Chenevert TL, Lawrence TS, Meyer CR, Johnson TD, Dong Q, Tsien C, Mukherji S, Quint DJ, Gebarski SS, et al. (2005). Functional diffusion map: a noninvasive MRI biomarker for early stratification of clinical brain tumor response. *Proc Natl Acad Sci USA* **102**, 5524–5529.

[15] Moffat BA, Chenevert TL, Meyer CR, McKeever PE, Hall DE, Hoff BA, Johnson TD, Rehemtulla A, and Ross BD (2006). The functional diffusion map: an imaging biomarker for the early prediction of cancer treatment outcome. *Neoplasia* **8**, 259–267.

[16] Hamstra DA, Chenevert TL, Moffat BA, Johnson TD, Meyer CR, Mukherji SK, Quint DJ, Gebarski SS, Fan X, Tsien CI, et al. (2005). Evaluation of the functional diffusion map as an early biomarker of time-to-progression and overall survival in high-grade glioma. *Proc Natl Acad Sci USA* **102**, 16759–16764.

[17] Tchougounova E, Kastemar M, Bråsäter D, Holland EC, Westermark B, and Uhrbom L (2007). Loss of Arf causes tumor progression of PDGFB-induced oligodendroglioma. *Oncogene* **26**, 6289–6296.

[18] Pitter KL, Galbán CJ, Galbán S, Saeed-Tehrani O, Li F, Charles N, Bradbury MS, Becher OJ, Chenevert TL, Rehemtulla A, et al. (2011). Perifosine and CCI 779 co-operate to induce cell death and decrease proliferation in PTEN-intact and PTEN-deficient PDGF-driven murine glioblastoma. *PLoS One* **6**, e14545.

[19] Ellingson BM, Malkin MG, Rand SD, Connelly JM, Quinsey C, LaViolette PS, Bedekar DP, and Schmainda KM (2010). Validation of functional diffusion maps (fDMs) as a biomarker for human glioma cellularity. *J Magn Reson Imaging* **31**, 538–548.

[20] Meyer CR, Boes JL, Kim B, Bland PH, Zasadny KR, Kison PV, Koral K, Frey KA, and Wahl RL (1997). Demonstration of accuracy and clinical versatility of mutual information for automatic multimodality image fusion using affine and thin-plate spline warped geometric deformations. *Med Image Anal* **1**, 195–206.

[21] Galbán CJ, Chenevert TL, Meyer CR, Tsien C, Lawrence TS, Hamstra DA, Junck L, Sundgren PC, Johnson TD, Ross DJ, et al. (2009). The parametric response map is an imaging biomarker for early cancer treatment outcome. *Nat Med* **15**, 572–576.

[22] Ellingson BM, Cloughesy TF, Zaw T, Lai A, Nghiemphu PL, Harris R, Lalezari S, Wagle N, Naeini KM, Carrillo J, et al. (2012). Functional diffusion maps (fDMs) evaluated before and after radiochemotherapy predict progression-free and overall survival in newly diagnosed glioblastoma. *Neuro Oncol* **14**, 333–343.

[23] Hamstra DA, Galbán CJ, Meyer CR, Johnson TD, Sundgren PC, Tsien C, Lawrence TS, Junck L, Ross DJ, Rehemtulla A, et al. (2008). Functional diffusion map as an early imaging biomarker for high-grade glioma: correlation with conventional radiologic response and overall survival. *J Clin Oncol* **26**, 3387–3394.

[24] Chung C, Jalali S, Foltz W, Burrell K, Wildgoose P, Lindsay P, Graves C, Camphausen K, Milosevic M, Jaffray D, et al. (2013). Imaging biomarker dynamics in an intracranial murine glioma study of radiation and antiangiogenic therapy. *Int J Radiat Oncol Biol Phys* **85**, 805–812.

[25] Chenevert TL, McKeever PE, and Ross BD (1997). Monitoring early response of experimental brain tumors to therapy using diffusion magnetic resonance imaging. *Clin Cancer Res* **3**, 1457–1466.

[26] Rehemtulla A (2012). Overcoming intratumor heterogeneity of polygenic cancer drug resistance with improved biomarker integration. *Neoplasia* **14**, 1278–1289.

[27] Lee KC, Hall DE, Hoff BA, Moffat BA, Sharma S, Chenevert TL, Meyer CR, Leopold WR, Johnson TD, Mazurchuk RV, et al. (2006). Dynamic imaging of emerging resistance during cancer therapy. *Cancer Res* **66**, 4687–4692.

[28] Reischauer C, Froehlich JM, Koh DM, Graf N, Padevit C, John H, Binkert CA, Boesiger P, and Gutzeit A (2010). Bone metastases from prostate cancer: assessing treatment response by using diffusion-weighted imaging and functional diffusion maps—initial observations. *Radiology* **257**, 523–531.

[29] Lee KC, Bradley DA, Hussain M, Meyer CR, Chenevert TL, Jacobson JA, Johnson TD, Galban CJ, Rehemtulla A, Pienta KJ, et al. (2007). A feasibility study evaluating the functional diffusion map as a predictive imaging biomarker for detection of treatment response in a patient with metastatic prostate cancer to the bone. *Neoplasia* **9**, 1003–1011.

[30] Loveless ME, Lawson D, Collins M, Nadella MV, Reimer C, Huszar D, Halliday J, Waterton JC, Gore JC, and Yankeelov TE (2012). Comparisons of the efficacy of a Jak1/2 inhibitor (AZD1480) with a VEGF signaling inhibitor (cediranib) and sham treatments in mouse tumors using DCE-MRI, DW-MRI, and histology. *Neoplasia* **14**, 54–64.

[31] Lee KC, Sud S, Meyer CR, Moffat BA, Chenevert TL, Rehemtulla A, Pienta KJ, and Ross BD (2007). An imaging biomarker of early treatment response in prostate cancer that has metastasized to the bone. *Cancer Res* **67**, 3524–3528.